Reduction of Rotor Vibration in Passively Stabilized Direction in Single-Drive Bearingless Motor

Hiroya Sugimoto [a], Seiyu Tanaka [a], and Akira Chiba [a]

[a] Tokyo Institute of Technology, 2-12-1 Ookayama, Meguro, Tokyo, Japan, sugimoto@belm.ee.titech.ac.jp

Abstract— **In this paper, an improvement of the rotor vibration in one-axis actively positioned single-drive bearingless motor (SDBM) with repulsive passive magnetic bearings is presented. The SDBM has only one set of three-phase windings. It generates both torque and active axial force independently driven by only one three-phase inverter and one displacement sensor. Therefore, the single-drive bearingless motors have the advantages of low cost and small size. Only axial *z*-axis is actively positioned. The other axes, radial movements *x* and *y*, and tilting movements θ_x and θ_y, are passively stable. Therefore, in the one degree-of-freedom (1DOF) bearingless motor, vibrations in the radial and tilting directions are serious problem. In this paper, an improvement method of the radial vibration in the 1DOF SDBM is presented. The principle of the radial vibration generation is shown. In the experiment, it is found that a correction of the rotor rotational angular position is effective for the radial vibration reduction.**

I. INTRODUCTION

Bearingless motors have advantages of no wear, no lubricant, non-pollution and maintenance-free because a magnetic bearing function is magnetically integrated in a single motor. Therefore, the bearingless motors have been applied in centrifugal pumps, contamination-free ventricular assist devices, high purity pharmaceutical mixing devices, rotating stages and flywheels.

In general magnetic suspension, five degree-of-freedom is actively positioned, however, for cost reduction, two degree-of-freedom (translational directions *x*, *y*) are actively positioned in the bearingless motor. On the other hands, in recent years, one degree-of-freedom (1DOF) bearingless motors have been studied because of the further cost reduction and down-sizing [1]-[7]. In the 1DOF bearingless motor, only the axial direction is actively positioned, thus, the cost is extremely low because only one displacement sensor and one or two inverters are necessary. The other radial and tilting directions are passively stabilized by passive magnetic bearings (PMB). The PMB is classified to attractive and repulsive types. In case of the attractive type PMBs in [1]-[3], the PMB is composed of the rotor permanent magnets and stator core, thus, the PMB functions are sometimes included in the bearingless motor structure. In case of the repulsive type in [4]-[7], additional two passive magnetic bearings are installed at both shaft ends of the bearingless motor in tandem. Improvement of the passive stiffness of the PMB is important because of the vibration reductions in the radial and tilting directions.

In the literatures, the rotor vibrations in the passively stable directions are reported [5], [7] and [8]. The vibration is increased at the critical speed, and in the worst case, the rotor is touch down. Most of the critical speed in the 1DOF bearingless motor is several thousand r/min. The authors have proposed a 1DOF single-drive bearingless motor (SDBM) with the repulsive passive magnetic bearing (RPMB) [9]. The critical speeds in the radial and tilting directions are improved because of high stiffness. However, the radial vibration is amplified around several thousand r/min.

In this paper, reduction of the radial vibration in a proposed 1DOF SDBM is presented. Two factors of the radial vibration generation are shown. The rotor angular position error results in the radial vibration because of interference between the axial and radial directions. A harmonic component in flux density in the air-gap also causes the radial vibration. Two rotors are fabricated and compared with respect to the flux density and radial vibration. It is found that a correction of the rotor rotational angular position and reduction of the harmonic component in the air-gap flux density are important for reducing the radial vibration.

II. STRUCTURE AND PRINCIPLE OF RADIAL VIBRATION

A. Structure of Proposed Single-Drive Bearingless Motor

Fig. 1 illustrates *xz* cross-sectional view of one of the representative single-drive bearingless motors. The single-drive bearingless motor (SDBM) is installed in the center, and the repulsive passive magnetic bearings (RPMBs) are installed at both ends of the SDBM. Each RPMB is constructed with the two permanent magnets. Four ring-shaped permanent-magnets are faced so that the radial stiffness is improved. The displacement sensor and the hall sensors are installed in the right and left end of the shaft, respectively. In the design, the radial air-gap length is 1 mm. In the SDBM part, only axial

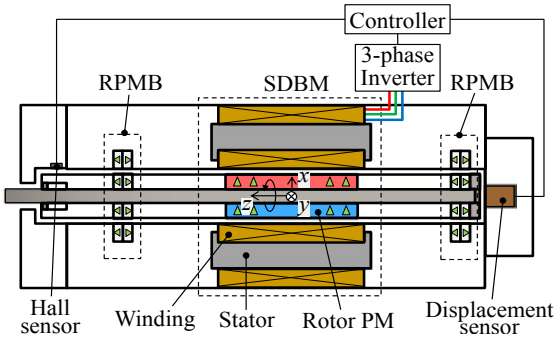

Fig. 1. System configuration of the proposed single-drive bearingless motor.

direction is actively positioned and the rotational torque is regulated, thus, only one displacement sensor and one three-phase inverter are necessary. Significant cost down can be realized.

Fig. 2 shows the detail of the winding structure of the proposed SDBM. Only one set of 3-phase 2-pole winding is installed. Fig. 2 shows the *xy* cross-sectional view. The windings are wound around the six stator cores. The black arrows in the windings indicate the positive current direction. Only the active axial force is generated by the *x*-*y* windings. To generate the rotating torque around *z*-axis, the current component in the *z*-axis is necessary. The torque by the Lorentz force is generated by the current component perpendicular to the current direction as the circle and cross marks shown in Fig. 2. The winding arrangement is similar to two-pole concentrated winding structure by a proposed V-shaped winding presented in [9]. Therefore, the rotating torque can be generated by the *q*-axis current i_q.

B. *Principle of Active Axial Force Generation*

Figs. 3(a) and 3(b) show principle of the active axial force generation. Fig. 3(a) shows the principle of the Maxwell force generation. The stator teeth are constructed to face to the air-gap. In addition, the stator core is composed of the six bars so that the permanent magnet fluxes at both rotor ends are circulated in the air-gap as shown by red arrows in Fig. 3(a). The suspension flux mainly flows in the air-gap in the *z*-direction. When the suspension flux is superimposed on the permanent magnet flux as shown in Fig. 3(a), the flux strengthening and weakening occur in the air-gaps at both axial ends. Therefore, the axial suspension force is generated in the positive *z*-direction. Fig. 3(b) shows the principle of the Lorentz force generation. At the rotor center in the *z*-direction, the permanent magnet fluxes go across the inside conductors confronting the air-gap. When the *d*-axis current is provided in the direction as indicated in Fig. 3(b), the Lorentz force is generated in the negative *z*-direction in the conductors. Thus, the active axial force is generated in the rotor in the positive *z*-direction as the counteractive force. The active axial force is a sum of the Maxwell and the Lorentz forces. On the other hand, when there is an error of the rotor rotational angular position, undesirable vibration occurs in the passive stabilized directions.

C. *Principle of Radial Vibration Generation*

Fig. 4 shows one of the factors in the axial vibration generation. In theoretical calculation, the axial force is not generated even if the *q*-axis current is excited. However, when there is an error between the actual and calculated rotor rotational angular positions, unfortunately, undesired axial force is generated because the *d*-axis current component is generated. In Fig. 4, the error angle is defined as θ_e. d_e-axis is shifted from *d*-axis by angle of θ_e. When i_{de} and i_{qe} are defined as currents on d_e- and q_e-axis, *d*- and *q*-axis currents i_d and i_q are given as

$$\begin{bmatrix} i_d \\ i_q \end{bmatrix} = \begin{bmatrix} \cos\theta_e & \sin\theta_e \\ -\sin\theta_e & \cos\theta_e \end{bmatrix} \begin{bmatrix} i_{de} \\ i_{qe} \end{bmatrix}. \quad (1)$$

Therefore, even when i_{de} is zero, i_d is not zero as shown in the following expression.

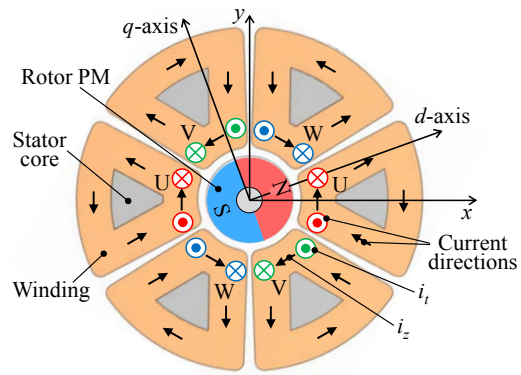

Fig. 2. *xy* cross-sectional view of the proposed SDBM.

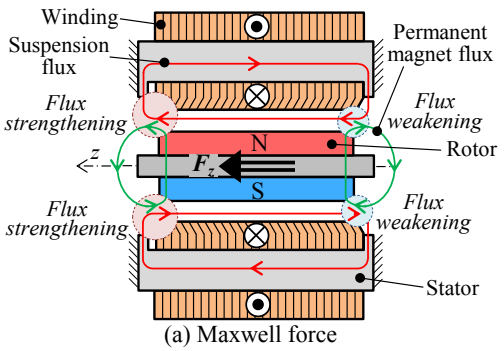

(a) Maxwell force

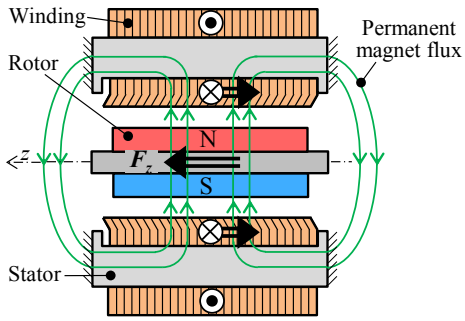

(b) Lorentz force

Fig. 3. Principle of the active axial force generation.

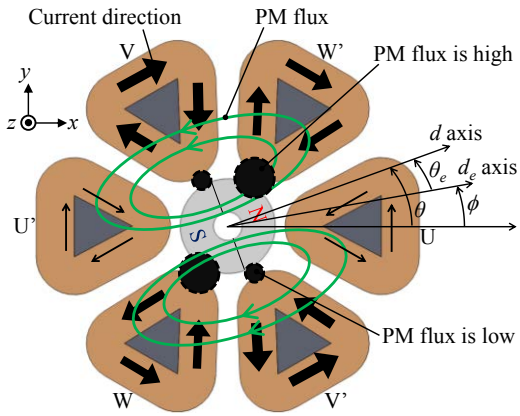

Fig. 4. Axial force generation because of the error angle.

$$\begin{bmatrix} i_d \\ i_q \end{bmatrix} = \begin{bmatrix} cos\theta_e & sin\theta_e \\ -sin\theta_e & cos\theta_e \end{bmatrix} \begin{bmatrix} 0 \\ i_{qe} \end{bmatrix} = \begin{bmatrix} i_{qe} sin\theta_e \\ i_{qe} cos\theta_e \end{bmatrix}. \quad (2)$$

The axial force is proportional to the *d*-axis current. When the error angle is equal to zero, the current-force coefficient is k_{zi}. The coefficient k_{zi} is varied with the error angle as sinusoidal waveform. Therefore, the undesired axial force F_{zd} is expressed as

$$F_{zd} = k_{zi} cos\theta_e i_d. \quad (3)$$

By substituting (2) into (3), F_{zd} is derived as follows:

$$F_{zd} = \frac{1}{2} k_{zi} i_{qe} sin2\theta_e. \quad (4)$$

In addition, the angular position error is varied with respect to the rotor rotational angular position. Therefore, the variation of the angular position error results in a disturbance, thus, the rotor is vibrated in the axial direction.

Fig. 5 shows the radial stiffness with respect to the rotor axial position. In the proposed structure, the positive radial stiffness is generated in the repulsive passive magnetic bearings. The radial stiffness is the highest at the aligned position between the rotor and stator permanent magnets. On the other hand, when the rotor is displaced in the positive or negative axial direction, the radial stiffness is reduced. Therefore, the radial stiffness is varied with twice frequencies with respect to the axial vibration. The variation of the radial stiffness results in movement of the radial position, thus, the radial vibration is generated. Thus, when the rotor is set in the aligned position as shown in Fig. 5, the second-order harmonic radial vibration occurs because of first-order axial vibration. The resonance between the second-order harmonic vibration and the natural frequency in the radial direction is serious problem. Thus, the axial vibration reduction by minimization of the angular position error is very important.

III. Test Results

Figs. 6(a) and 6(b) show rotor 1 and rotor 2, respectively. Rotor permanent magnet installed at center is magnetized in two-pole parallel direction. Two repulsive passive magnetic bearings are magnetized in thrust direction. The shaft diameters of rotor 1 and rotor 2 are 3 mm and 5 mm, respectively. Two sensor targets for monitoring radial direction are slightly different. The diameter in the rotor 2 is decreased for reduction of the rotor mass. However, the rotor outer diameters are both 10 mm. In addition, dimensions of the rotor PM and RPMBs are exactly identical. The PM and shaft materials are Nd-Fe-B and stainless, respectively. The rest spaces at both side of the rotor PM are necessary to avoid interference between the rotor PM and the RPMBs.

Fig. 7 shows spectrum of the radial displacement when an impulse disturbance is applied in the rotor shaft end in the radial direction. The rotor radial movement is measured by two displacement sensors. The rotor is vibrated by the impulse disturbance. The radial natural frequencies of rotor 1 and rotor 2 are 85.4 Hz and 79.4 Hz, respectively. Therefore, critical speeds may be 5124 r/min and 4758 r/min. In the impulse disturbance test, amplitude of the radial displacement is not important, but rather the natural frequency is significant result for calculating a radial stiffness.

Table I shows radial stiffness of rotor 1 and rotor 2. When the rotor mass is m and the natural frequency is f_n, the radial stiffness k_r is given by

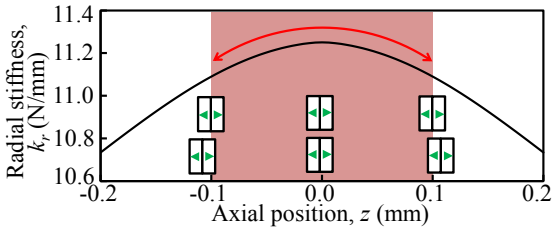

Fig. 5. Radial stiffness with respect to the axial position.

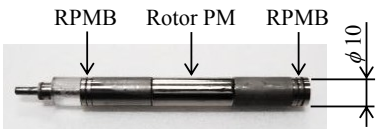

(a) Rotor 1.

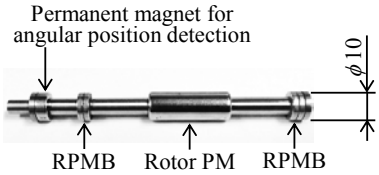

(b) Rotor 2

Fig. 6. Fabricated rotors.

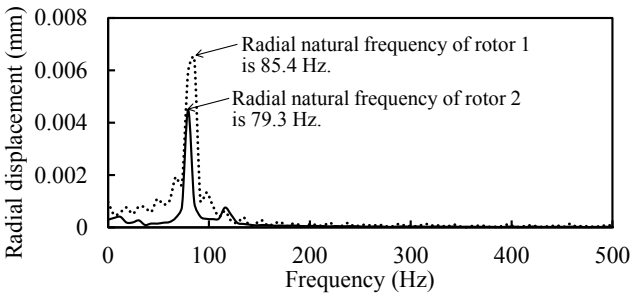

Fig. 7. Spectrum of radial displacement when an impulse disturbance is applied in rotor shaft end.

TABLE I RADIAL STIFFNESS OF TWO ROTORS.

	Rotor mass	Radial natural frequency	Radial stiffness
Rotor 1	0.039 kg	85.4 Hz	11.2 N/mm
Rotor 2	0.038 kg	79.3 Hz	9.4 N/mm

$$k_r = m(2\pi f_n)^2. \quad (5)$$

From expression (5), the radial stiffness of rotor 1 and rotor 2 are 11.2 N/mm and 9.4 N/mm, respectively. The radial stiffness of rotor 2 is low compared with that of rotor 1 because flux density in the air-gap is decreased. In the case of rotor 2, the shaft diameter is extended for enhancement of the shaft stiffness. Therefore, radial thickness of rotor permanent magnets is decreased so that permanent magnet flux is reduced.

Fig. 8 shows the angular position error with respect to the rotor rotational angular position. The angular position is calculated by linearized equation every 90 degrees. Before

correction of the angular position in rotor 1, the maximum error is 7.1 degrees. On the other hand, after the gain and offset in the linearized equation are improved, the maximum error is reduced by 1.9 degrees. In the case of rotor 2, maximum error angle is 1.7 degrees. Therefore, it is expected that axial and radial vibrations in rotor 1 with angular position correction and rotor 2 are reduced compared with rotor 1 without angular position correction.

Fig. 9(a) shows harmonic order components in the error angle with respect to rotor 1 without angular position correction. Second-order component is the highest. When the rotor is rotated at constant angular speed ω, the second-order component in the error angle causes axial vibration of second-order 2ω. As a result, the second-order axial vibration generates radial vibration of fourth-order 4ω. After angular position correction, the second-order component is reduced by 89 % as shown in Fig. 9(b). Error angle in rotor 2 is also corrected so that the second-order component is reduced as shown in Fig. 9(c). However, the first- and second-order components are slightly increased compared with Fig. 9(b).

Fig. 10(a) and 10(b) show ratio of harmonic order component in surface flux density in the axial direction with respect to RPMBs in rotor 1 and rotor 2. The surface flux densities in the axial direction at positions a, b, c and d are measured. The measured four positions are indicated in Fig. 10(a) and 10(b). Ideally, the surface flux density is constant. However, in the fabricated RPMBs, harmonic components are included because of magnetization error. In the surface flux density of RPMBs in rotor 1, second-order harmonic component is high compared with first-order component. Therefore, in the case of rotor 1, second-order radial vibration may be increased. On the other hand, in the case of rotor 2, first-order component is high compared with second-order harmonic component. Thus, radial vibration synchronized a rotational speed may be increased.

Fig. 11 shows the radial displacement of rotor 1 before/after the correction of the rotor rotational angular position and that of rotor 2. The touch down length in the radial direction is 0.3 mm. Before the correction, the rotor is touch down in the radial direction at around 1600 r/min. On the other hand, after the angular position correction, the rotor radial vibration is reduced, thus, the rotational speed is improved up to 2200 r/min. However, when the rotational speed is around 2200 r/min, the rotor radial vibration is increased, and then, the rotor is touch down. In the case of rotor 2, radial vibration is higher than rotor 1 with the angular position correction at low speed because the radial stiffness is lower than rotor 1. However, rotor 2 can rotate without touch down at 2300 r/min because second-order harmonic components in the error angle and flux density in the air-gap are decreased. In the experiments, two valuable results are confirmed. Firstly, when radial stiffness is increased, the radial vibration is decreased. Secondly, it is found that reductions of the second-order harmonic component in the error angle and in the flux density generated by the RPMBs are important for reducing radial vibration.

ACKNOWLEDGMENT

This work was supported by JSPS KAKENHI Grant Number 24246046.

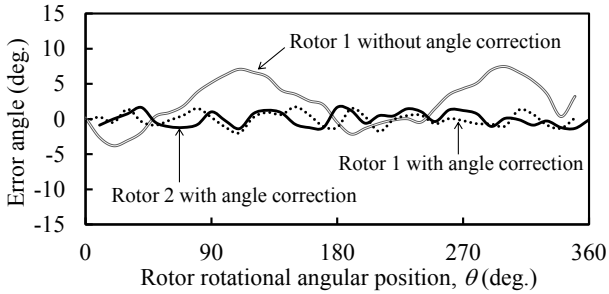

Fig. 8 Angular position error with respect to the rotor rotational angular position.

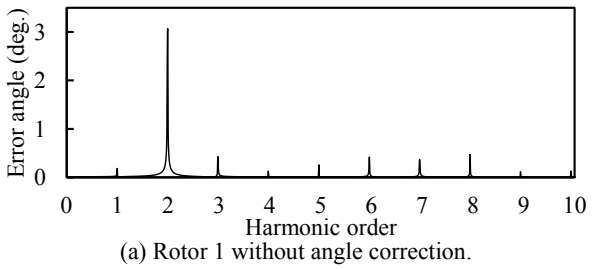

(a) Rotor 1 without angle correction.

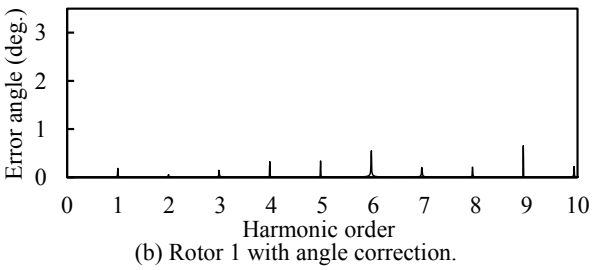

(b) Rotor 1 with angle correction.

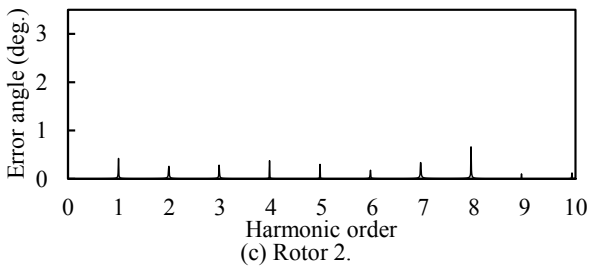

(c) Rotor 2.

Fig. 9 Harmonic order components in error between an actual and calculated rotational angular positions.

IV. CONCLUSION

This paper presents reduction of the radial vibration in a proposed 1DOF single-drive bearingless motor. In the experiments, two factors of the radial vibration generation are shown. The rotor angular position error results in the radial vibration because of interference between the axial and radial directions. A harmonic component in flux density in the air-gap also causes the radial vibration. It is found that a correction of the rotor rotational angular position and reduction of the harmonic component in the air-gap flux density are important for reducing radial vibration. Moreover, when the radial stiffness is increased, the radial vibration is decreased.

REFERENCES

[1] I. D. Silva and O. Horikawa, “An attraction-type magnetic bearing with control in a single direction,” *IEEE Trans. Ind. Appl.*, vol. 36, no. 4, pp. 1138–1142, Jul./Aug. 2000.

[2] J. Kuroki, T. Shinshi, L. Li, and A. Shimokohbe, “Miniaturization of a one-axis-controlled magnetic bearing,” *Precis. Eng.*, vol. 29, no. 2, pp. 208–218, Apr. 2005.

[3] J. Asama, Y. Hamasaki, T. Oiwa, and A. Chiba, "A Novel Concept of a Single-Drive Bearingless Motor", *IEEE Trans. Industrial Electronics,* vol. 60, no. 1, pp. 129-138, Jan. 2013.

[4] Q. D. Nguen and S. Ueno, “Modeling and control of salient-pole permanent magnet axial-gap self-bearing motor,” *IEEE/ASME Trans. Mechatronics,* vol. 16, no. 3, pp. 518–526, Jun. 2011.

[5] S. Yang and M. Huang, “Design and Implementation of a Magnetically Levitated Single-Axis Controlled Axial Blood Pump”, *IEEE Trans. Industrial Electronics,* vol. 56, no. 6, pp. 2213-2219, Jun. 2009.

[6] W. Bauer and W. Amrhein, “Electrical design and winding selection for a bearingless Axial-Force/Torque Motor”, *in Proc. International Symposium on Power Electronics, Electrical Drives, Automation and Motion (SPEEDAM)*, pp. 1224-1229, 2012.

[7] T. Ohji, Y. Katsuda, K. Amei and M. Sakui, “Structure of One-Axis Controlled Repulsive Type Magnetic Bearing System With Surface Permanent Magnets Installed and Its Levitation and Rotation Tests,” *IEEE Trans. Magn*., vol. 47, no. 12, pp. 4734-4739, Dec. 2011.

[8] J. Asama, Y. Hamasaki, T. Oiwa, and A. Chiba, “Performance Improvement of a One-DOF Actively Positioned Bearingless Motor”, in *Proc. 13th Int. Symp. Magnetic Bearings*, 2012.

[9] H. Sugimoto, S. Tanaka, A. Chiba, and J. Asama, “Design and Test Result of Novel Single-Drive Bearingless Motor with Cylindrical Radial Gap”, *in Proc. Energy Convers. Congr. and Expo. (ECCE)*, pp. 2466-2473, 2013.

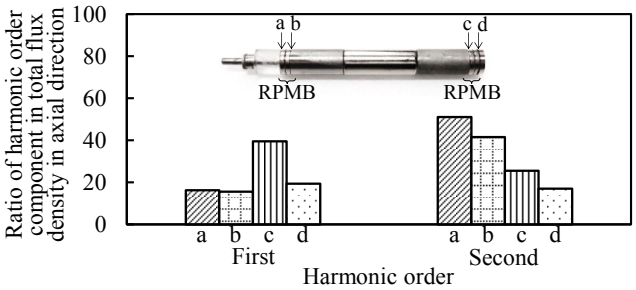

(a) Rotor 1.

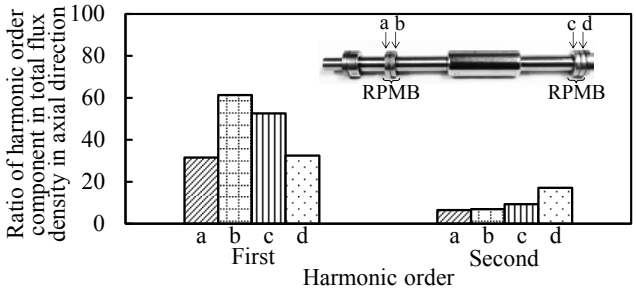

(b) Rotor 2.

Fig. 10 Harmonic order components in surface flux density on repulsive passive magnetic bearings.

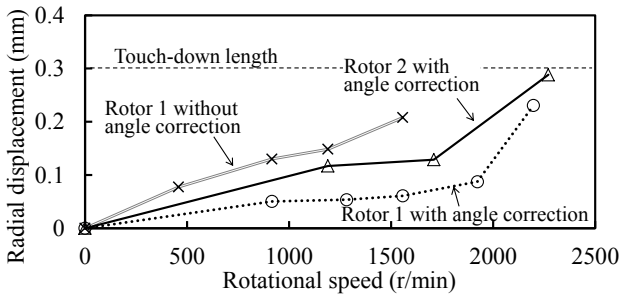

Fig. 11. Radial displacement with respect to rotational speed.